

## Trapping an Intermediate of Dinitrogen (N<sub>2</sub>) Reduction on Nitrogenase<sup>†</sup>

Brett M. Barney,<sup>‡</sup> Dmitriy Lukoyanov,<sup>||</sup> Robert Y. Igarashi,<sup>‡,⊥</sup> Mikhail Laryukhin,<sup>||</sup> Tran-Chin Yang,<sup>||</sup>  
Dennis R. Dean,<sup>§</sup> Brian M. Hoffman,<sup>\*,||</sup> and Lance C. Seefeldt<sup>\*,‡</sup>

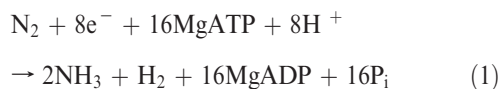
<sup>‡</sup>Department of Chemistry and Biochemistry, Utah State University, Logan, Utah 84322, <sup>§</sup>Department of Biochemistry, Virginia Tech, Blacksburg, Virginia 24061, and <sup>||</sup>Department of Chemistry, Northwestern University, Evanston, Illinois 60208.

<sup>⊥</sup>Present address: Department of Chemistry, University of Central Florida, Orlando, FL 32816.

Received June 29, 2009; Revised Manuscript Received August 10, 2009

**ABSTRACT:** Nitrogenase reduces dinitrogen (N<sub>2</sub>) by six electrons and six protons at an active-site metal-locus called FeMo cofactor, to yield two ammonia molecules. Insights into the mechanism of substrate reduction by nitrogenase have come from recent successes in trapping and characterizing intermediates generated during the reduction of protons as well as nitrogenous and alkyne substrates by MoFe proteins with amino acid substitutions. Here, we describe an intermediate generated at a high concentration during reduction of the natural nitrogenase substrate, N<sub>2</sub>, by wild-type MoFe protein, providing evidence that it contains N<sub>2</sub> bound to the active-site FeMo cofactor. When MoFe protein was frozen at 77 K during steady-state turnover with N<sub>2</sub>, the  $S = 3/2$  EPR signal ( $g = [4.3, 3.64, 2.00]$ ) arising from the resting state of FeMo cofactor was observed to convert to a rhombic,  $S = 1/2$ , signal ( $g = [2.08, 1.99, 1.97]$ ). The intensity of the N<sub>2</sub>-dependent EPR signal increased with increasing N<sub>2</sub> partial pressure, reaching a maximum intensity of approximately 20% of that of the original FeMo cofactor signal at  $\geq 0.2$  atm N<sub>2</sub>. An almost complete loss of resting FeMo cofactor signal in this sample implies that the remainder of the enzyme has been reduced to an EPR-silent intermediate state. The N<sub>2</sub>-dependent EPR signal intensity also varied with the ratio of Fe protein to MoFe protein (electron flux through nitrogenase), with the maximum signal intensity observed with a ratio of 2:1 (1:1 Fe protein:FeMo cofactor) or higher. The pH optimum for the signal was 7.1. The N<sub>2</sub>-dependent EPR signal intensity exhibited a linear dependence on the square root of the EPR microwave power in contrast to the nonlinear response of signal intensity observed for hydrazine-, diazene-, and methyldiazene-trapped states. <sup>15</sup>N ENDOR spectroscopic analysis of MoFe protein captured during turnover with <sup>15</sup>N<sub>2</sub> revealed a <sup>15</sup>N nuclear spin coupled to the FeMo cofactor with a hyperfine tensor  $A = [0.9, 1.4, 0.45]$  MHz establishing that an N<sub>2</sub>-derived species was trapped on the FeMo cofactor. The observation of a single type of <sup>15</sup>N-coupled nucleus from the field dependence, along with the absence of an associated exchangeable <sup>1</sup>H ENDOR signal, is consistent with an N<sub>2</sub> molecule bound end-on to the FeMo cofactor.

Nitrogenase catalyzes the reduction of dinitrogen (N<sub>2</sub>), yielding two ammonia molecules in a reaction requiring protons, electrons, and MgATP with an ideal stoichiometry (eq 1) (1–4):



For the Mo-dependent nitrogenase, N<sub>2</sub> binding and reduction occur at a complex metal cluster called the FeMo cofactor<sup>1</sup> ([7Fe-9S-Mo-homocitrate-X]) bound within the MoFe protein (5–7). The Fe protein delivers electrons to the MoFe protein in a reaction requiring the hydrolysis of a minimum of two MgATP molecules per electron transferred (1). Following each electron transfer, the oxidized Fe protein dissociates from the MoFe

protein, with the cycle being repeated until sufficient electrons have accumulated within the MoFe protein to carry out substrate reduction (8). In the absence of any other substrate, nitrogenase catalyzes the reduction of protons, yielding H<sub>2</sub> (9). When N<sub>2</sub> is present, electrons flowing through nitrogenase are partitioned into the reduction of N<sub>2</sub> and protons, with a minimum of one H<sub>2</sub> molecule formed to one N<sub>2</sub> molecule reduced (10). One of the significant unknowns about nitrogenase remains a molecular-level understanding of the substrate reduction mechanism.

Over recent years, some insights into the nitrogenase mechanism have been gained by combining three experimental strategies: (i) the substitution of specific amino acids within the MoFe protein, (ii) freeze trapping substituted MoFe proteins during turnover using different substrates, and (iii) characterization of the resulting trapped state by paramagnetic resonance methods (2). The substitution of amino acids within the MoFe protein has been guided by examination of the X-ray structure of the MoFe protein (7, 11–13) and by genetic studies (14–16) and has been focused on residues located near the FeMo cofactor (e.g.,  $\alpha$ -70<sup>Val</sup> and  $\alpha$ -195<sup>His</sup>). Substrates that have been trapped on substituted MoFe proteins include protons, acetylene (HC≡CH), hydrazine (H<sub>2</sub>N–NH<sub>2</sub>), diazene (HN=NH), methyldiazene (HN=N–CH<sub>3</sub>), propargyl alcohol (HC≡C–CH<sub>2</sub>OH), and carbonyl disulfide (CS<sub>2</sub>) (2).

<sup>†</sup>This work was supported by grants from the National Institutes of Health (R01-GM59087 to L.C.S. and D.R.D. and HL13531 to B.M.H.) and the National Science Foundation (MCB-0723330 to B.M.H.).

\*To whom correspondence should be addressed. L.C.S.: phone, (435) 797-3964; fax, (435) 797-3390; e-mail, seefeldt@cc.usu.edu. B.M.H.: phone, (847) 491-3104; fax, (847) 491-7713; e-mail, bmh@northwestern.edu.

<sup>1</sup>Abbreviations: FeMo cofactor, iron–molybdenum cofactor; EPR, electron paramagnetic resonance; ENDOR, electron nuclear double resonance.

For each of these trapped states, a unique EPR-active state of the FeMo cofactor is observed, allowing characterization of the trapped complex by EPR and ENDOR spectroscopies. Through the use of substrate isotopomers, such studies have provided insights into the nature of several of the bound substrate-derived species (3). For example, it was deduced that a state trapped during reduction of propargyl alcohol contained the two-electron reduced allyl alcohol product whose terminal alkene is bound side-on to a metal ion of the FeMo cofactor that was assigned as an Fe ion (17); a similar binding geometry was deduced for a trapped acetylene reduction intermediate (18). The state trapped during turnover under Ar can be best described as two hydrides bound to the FeMo cofactor (19) and subsequently was shown by a step-annealing relaxation protocol to be a state of the MoFe protein that has accumulated four electrons (and presumably protons) relative to resting MoFe protein (20), denoted  $E_4$  by Lowe and Thorneley (21). The species bound during reduction of the nitrogenous substrates, hydrazine, diazene, and methyldiazene, all were shown by a combination of  $^{14/15}\text{N}$  and  $^1\text{H}$  ENDOR spectroscopy to contain a substrate-derived ( $-\text{NH}_x$ ) moiety bound to the FeMo cofactor (3).

Studies completed to date have relied on MoFe proteins having amino acid substitutions and using nonphysiological substrates (2, 3). To directly address the  $\text{N}_2$  reduction mechanism, it would be desirable to trap the wild-type MoFe protein during turnover with the physiological substrate  $\text{N}_2$  in a state that would be amenable to characterization by spectroscopic methods. Earlier, we reported preliminary evidence that an intermediate could be trapped during  $\text{N}_2$  reduction in the wild-type MoFe protein (22). Here, we report conditions for optimization of a  $\text{N}_2$ -trapped state in the wild-type MoFe protein and present a characterization of this trapped state by EPR and  $^{15}\text{N}$  and  $^{1,2}\text{H}$  ENDOR spectroscopic methods.

## MATERIALS AND METHODS

**Materials and Protein Purification.** All reagents were obtained from Sigma-Aldrich (St. Louis, MO) and were used as provided unless specified otherwise.  $^{15}\text{N}$ -labeled dinitrogen was obtained from Cambridge Isotope Laboratories. Nitrogenase MoFe protein was purified from *Azotobacter vinelandii* strain DJ995 and Fe protein from strain DJ884 as previously described (23). The MoFe protein, expressed with a seven-histidine tag near the C-terminus of the  $\alpha$ -subunit, was purified by a metal affinity chromatography protocol (23). Proteins were greater than 95% pure as judged by SDS-PAGE with Coomassie blue staining. Protein concentrations were determined by the Biuret method with bovine serum albumin as the standard. All manipulation of proteins was done in septum-sealed serum vials under an argon atmosphere, and gas and liquid transfers were conducted with gastight syringes.

**Substrate Reduction.** The rates for substrate reduction were determined in 9 mL sealed vials with a liquid volume of 1 mL as described previously (24), with a total assay time of 10 min at 30 °C. The assay mixture contained a MgATP regeneration system (5 mM ATP, 6 mM  $\text{MgCl}_2$ , 30 mM phosphocreatine, 0.2 mg/mL creatine phosphokinase, and 1.2 mg/mL bovine serum albumin) in a 200 mM MOPS buffer (pH 7.1) with 9 mM sodium dithionite. Dioxygen was removed from all solutions by evacuation and refilling with argon. MoFe protein was added (100  $\mu\text{g}$ ) followed by Fe protein (500  $\mu\text{g}$ ) to initiate the reaction. Reactions were quenched by the addition of 300  $\mu\text{L}$  of a 400 mM EDTA solution. For experiments with less than 1 atm of

$\text{N}_2$ , the  $\text{N}_2$  was added as an overpressure to an argon-filled assay vial followed by venting the vial to atmospheric pressure. The  $\text{N}_2$  in each vial was quantified by analysis of an aliquot of the gas phase by gas chromatography. For experiments at 1 atm of  $\text{N}_2$ , the vial was evacuated and refilled with  $\text{N}_2$  from the manifold, followed by venting to 1 atm. When the Fe protein to MoFe protein ratio was varied, the amount of MoFe protein was maintained at 100  $\mu\text{g}$  while the amount of Fe protein was varied between 12.5  $\mu\text{g}$  and 250  $\mu\text{g}$ .

$\text{H}_2$  was quantified from the headspace of quenched vials by gas chromatography with a molecular sieve 5A column and a TCD detector. Ammonia was quantified by the fluorescence method described previously (24), with a standard curve prepared using  $\text{NH}_4\text{Cl}$ .

**X-Band EPR Sample Preparation and Analysis.** Samples under turnover conditions were prepared in a reaction mixture containing a MgATP regeneration system (10 mM ATP, 15 mM  $\text{MgCl}_2$ , 20 mM phosphocreatine, 0.3 mg/mL phosphocreatine kinase, and 2.6 mg/mL bovine serum albumin) in 150 mM MOPS buffer (pH 7.1 unless stated otherwise) with 50 mM sodium dithionite. The MoFe protein concentration was  $\sim 50 \mu\text{M}$  in all samples, and the reaction was initiated by the addition of 50  $\mu\text{M}$  Fe protein. The reaction was allowed to proceed for 15 s at room temperature in 4 mm calibrated quartz EPR tubes (Wilmaad, Buena, NJ) followed by emersion in a hexane/liquid  $\text{N}_2$  slurry. Resting-state samples were prepared as described above, except that Fe protein was not included.

For the pH profile, the same solution as described above was used, except that the buffer consisted of 50 mM MES, 50 mM TAPS, and 50 mM MOPS, with the pH adjusted by the addition of HCl or NaOH. When the ratio of Fe protein to MoFe protein was varied, the concentration of MoFe protein was maintained at 50  $\mu\text{M}$  while the concentration of Fe protein ranged between 25 and 200  $\mu\text{M}$ . When the partial pressure of  $\text{N}_2$  was varied,  $\text{N}_2$  gas was added to the argon-filled assay vial as an overpressure and then the vial was vented to 1 atm. For the 1 atm  $\text{N}_2$  sample, the sample vial and EPR tube were both evacuated and filled with  $\text{N}_2$  gas.

X-Band EPR spectra were recorded using a Bruker ESP-300 E spectrometer with an ER 4116 dual-mode X-band cavity equipped with an Oxford Instruments ESR-900 helium flow cryostat. Spectra were recorded at microwave frequencies near 9.65 GHz; precise values of the frequency were recorded for each spectrum. The microwave power dependence on EPR signal intensity was determined at 4.7 K with microwave powers from 5  $\mu\text{W}$  to 1 mW. The temperature dependence (4.7 to 12 K) of the EPR signal intensity was determined with the microwave power maintained at 50  $\mu\text{W}$ , a nonsaturating value at the lowest temperature.

Spin integration of the EPR signal intensity for the  $\text{N}_2$ -dependent state was accomplished by comparison to a 50  $\mu\text{M}$  copper EDTA standard, taking into account the correction for  $g$  value differences. Samples were compared at the same power, modulation amplitude, temperature, and number of scans. Integrations were done using IGOR Pro (WaveMetrics, Lake Oswego, OR).

**ENDOR Sample Preparation and Analysis.** ENDOR samples were prepared as described above, except that the final MoFe protein concentration was  $\sim 150 \mu\text{M}$  and the samples were frozen in Q-band tubes. CW and pulsed 35 GHz ENDOR spectra were recorded at 2 K on spectrometers described previously. In these experiments, the ENDOR pattern for a single orientation of

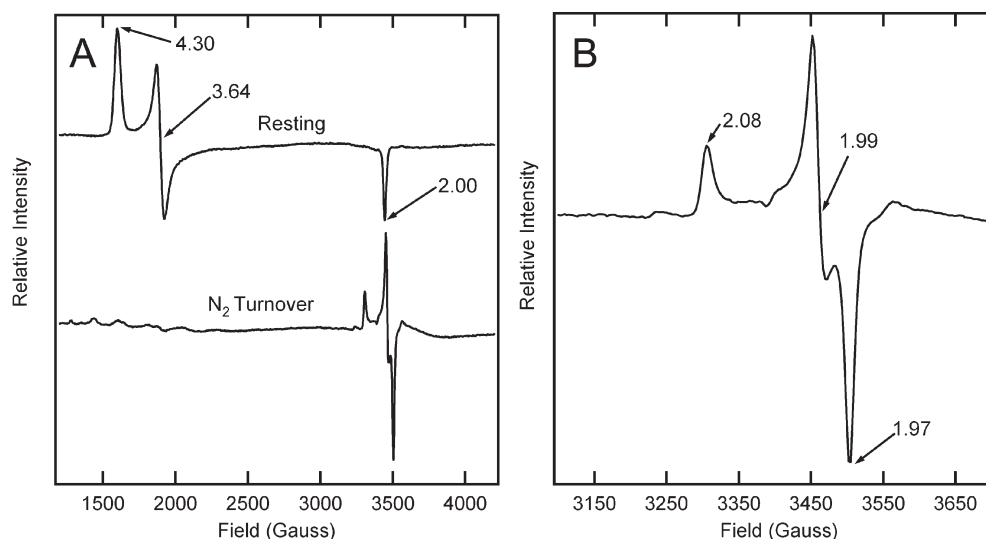


FIGURE 1: X-Band EPR spectra of nitrogenase. (A) X-Band EPR spectrum for the resting state of the MoFe protein (Resting) and of the MoFe protein trapped by being frozen to 77 K during turnover under 1 atm of N<sub>2</sub> (N<sub>2</sub> turnover). (B)  $g \sim 2$  region of the N<sub>2</sub> turnover-trapped state. The concentration of MoFe protein is 50  $\mu$ M. Turnover conditions are described in Materials and Methods and include 50  $\mu$ M Fe protein. The EPR microwave power was 1.0 mW, the temperature 4.8 K, and the modulation frequency 1.26 mT. Each trace is the sum of five scans.

an  $I = 1/2$  nucleus ( $^1\text{H}$ ,  $^{15}\text{N}$ ) exhibits a  $\nu(\pm)$  doublet that is split by the hyperfine coupling,  $A$ , and centered at the nuclear Larmor frequency. The Mims pulse ENDOR sequence,  $[\pi/2 - \tau - \pi/2 - T - (\text{rf}) - \pi/2 - \text{detect}]$ , was implemented with random hopping of the radiofrequency over the frequency range for a spectrum, a procedure that improves intensity and signal shape. This sequence has the property that its ENDOR intensities follow the relationship  $I(A) \sim 1 - \cos(2\pi A\tau)$ . As a result, the signals vanish ("blind spots") at  $A\tau = n$  ( $n = 0, 1, \dots$ ) and show maximum intensities at  $A\tau = n + 1/2$ . The full hyperfine tensor for an interacting nucleus is determined by analysis of a two-dimensional (2D) field-frequency pattern comprised of numerous spectra collected across the EPR envelope, as described previously (25).

## RESULTS

**Trapping an Intermediate during Reduction of N<sub>2</sub> by Wild-Type MoFe Protein.** The resting state of the FeMo cofactor in the MoFe protein occurs at  $S = 3/2$  and exhibits a characteristic low-temperature (2–8 K) EPR spectrum ( $g = [4.30, 3.64, 2.0]$ ) (Figure 1). When the MoFe protein is trapped by rapid freezing at 77 K during turnover under argon (in the presence of Fe protein, MgATP, a MgATP regeneration system, and dithionite), the resting-state FeMo cofactor  $S = 3/2$  EPR signal diminishes in intensity. This feature has been interpreted to result from reduction of the resting state of the FeMo cofactor (called the M<sup>N</sup> state) to one or more EPR-silent states (26). We now report that the MoFe protein can be trapped during turnover of the substrate N<sub>2</sub> in an EPR-active state of the FeMo cofactor having a novel  $S = 1/2$  rhombic EPR signal where  $g = [2.08, 1.99, 1.97]$  (Figure 1). As described below, the intensity of this new EPR signal is dependent on the pH of the reaction solution, the concentration of N<sub>2</sub>, the electron flux through nitrogenase, and the time and method of freeze trapping.

As shown in Figure 2, the intensity of the N<sub>2</sub>-dependent EPR signal progressively increases as the pH of the solution increases from 6.0 to 7.1, reaching an optimum at pH 7.1, and then gradually decreases as the pH of the solution increases from 7.1 to 8.4; pH values outside of 6.0 and 8.4 were not examined as the

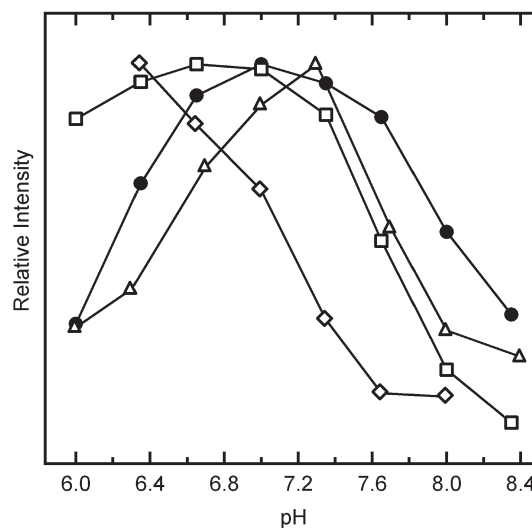


FIGURE 2: Dependence of EPR signal intensity on pH. Shown are the relative intensities of the EPR signals for the turnover-trapped states with N<sub>2</sub> (●), diazene (◇), hydrazine (△), and methyldiazene (□) as substrates. The EPR microwave power was 1.0 mW and the temperature 5.2 K. All other conditions are noted in Materials and Methods.

MoFe protein is not stable under these conditions. Earlier, conditions were established for trapping a MoFe protein having both  $\alpha$ -70<sup>Val</sup> substituted with alanine and  $\alpha$ -195<sup>His</sup> substituted with glutamine using the nitrogenous substrates hydrazine, diazene, or methyldiazene. The  $S = 1/2$  EPR signals of the trapped states are similar in line shape (22) but exhibit different  $g$  values compared to the N<sub>2</sub>-dependent EPR signal reported here. Figure 2 shows that the pH dependence of the intensity of the N<sub>2</sub>-dependent EPR signal is different from the pH dependences of the other trapped substrates. The hydrazine-trapped state showed the most similarity to the N<sub>2</sub>-dependent EPR signal, although it has a much narrower optimum around pH 7.6, while the diazene-trapped state stands out as having a curve that is shifted farthest to low pH and that increases to low pH without reaching a maximum. The differences in pH dependences for each of these EPR signals point to differences among the trapped states.



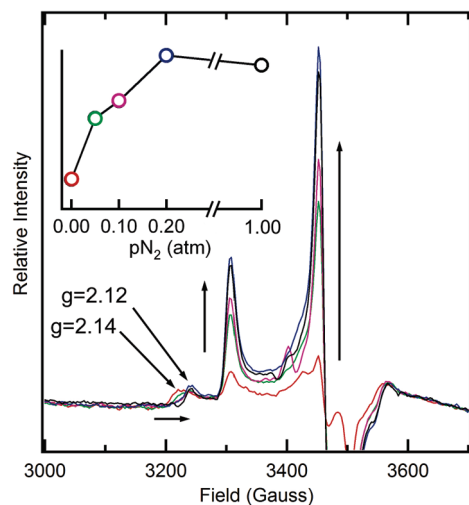


FIGURE 3: Dependence of EPR signal intensity on the partial pressure of  $N_2$ . EPR spectra ( $g \sim 2$  region) are shown of the MoFe protein trapped during turnover under different partial pressures of  $N_2$ , including 0 (red), 0.05 (green), 0.1 (magenta), 0.2 (blue), and 1 atm (black). The inset shows the relative intensity of the  $g = 1.99$  EPR signal as a function of the partial pressure of  $N_2$ . The EPR microwave power was 1.0 mW and the temperature 4.9 K. Other conditions are described in Materials and Methods.

As the partial pressure of  $N_2$  is increased, the intensity of the  $N_2$ -dependent EPR signal progressively increases, reaching a maximum value at a  $N_2$  partial pressure of 0.2 atm; it then remains constant up to 1 atm of  $N_2$  (Figure 3). The  $K_m$  for  $N_2$  reduction is around 0.1 atm (27, 28). Thus, the dependence of the  $N_2$ -dependent EPR signal on the  $N_2$  concentration matches well with the dependence of the substrate reduction rate on  $N_2$  concentration.

Under turnover conditions in the absence of  $N_2$ , a low-intensity EPR signal ( $g_1 = 2.14$ ) is observed that corresponds to the signal assigned to the  $E_4$  state (29). This inflection shifts to  $g = 2.12$  as the  $N_2$  partial pressure is increased, suggesting that  $N_2$  interacts with the FeMo cofactor of this state.

The rate of electron flow (electron flux) through nitrogenase can be controlled by the ratio of Fe protein to MoFe protein, with the highest flux at the highest ratios (30). Low electron flux (fewer than four Fe protein molecules per MoFe protein) is expected to result in population of the lower reduced states of the MoFe protein, termed the  $E_1$  and  $E_2$  states in the Thorneley and Lowe kinetic scheme (21). At higher flux (ratios of  $> 4:1$ ), more reduced states of the MoFe protein are populated ( $E_3$  and  $E_4$ ). The intensity of the  $N_2$ -dependent EPR signal was found to vary with the electron flux through nitrogenase, with a lower signal intensity at the lowest flux, as expected for  $N_2$  binding at  $E_3$  and  $E_4$ . Increasing electron flux resulted in an increase in the EPR signal intensity to an apparent plateau at a protein ratio of 4:1 (Figure 4). The intensity of the  $N_2$ -dependent EPR signal did not increase at higher electron flux. However, the signal becomes more difficult to observe at higher concentrations of Fe protein because it is masked by the  $S = 1/2$  EPR signal of the  $[4Fe-4S]^+$  state of the Fe protein, which is centered around  $g = 2$ .

It was important to establish that nitrogenase effectively reduces  $N_2$  to ammonia over the electron flux range that yields the  $N_2$ -dependent EPR signal. Figure 5 shows the dependence of the specific activity for  $N_2$  reduction on the ratio of Fe protein to MoFe protein. This specific activity continues to increase through the maximum ratio of 10:1, whereas the intensity of

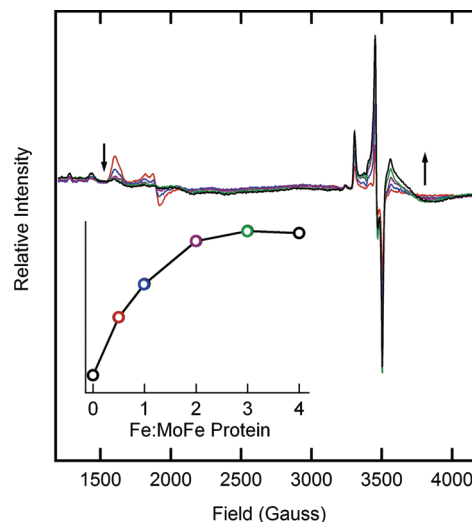


FIGURE 4: Dependence of EPR signal intensity on the electron flux through nitrogenase. EPR spectra ( $g \sim 2$  region) are shown for nitrogenase trapped during turnover of  $N_2$  with different ratios of Fe protein to MoFe protein, including 0.5:1 (red), 1:1 (blue), 2:1 (magenta), 3:1 (green), and 4:1 (black). The inset shows the relative intensity of the  $g = 1.99$  EPR signal as a function of the Fe protein: MoFe protein ratio. The EPR microwave power was 1.0 mW and the temperature 5.2 K. Other conditions are described in Materials and Methods.

the  $N_2$ -derived EPR intermediate plateaus at  $\sim 3\text{--}4:1$  (Figure 4). At an Fe protein:MoFe protein ratio of 1:1, the rate of  $N_2$  reduction still is approximately  $180 \text{ nmol of } NH_3 \text{ min}^{-1} (\text{mg of MoFe protein})^{-1}$ , or 30% of the maximal rate. This result demonstrates that dinitrogen is reduced at significant rates even when nitrogenase is turning over under conditions traditionally termed low flux ( $\leq 4:1$  ratio), and that the  $N_2$ -dependent EPR state trapped here thus represents a state that is actively reducing  $N_2$ .

In the absence of any other substrate, all of the electron flux through nitrogenase under Ar reduces protons to  $H_2$  (1). The specific activity for this  $H_2$  formation also increases with increasing electron flux through nitrogenase up to a maximum proton reduction rate at a ratio Fe protein:MoFe protein of 10:1, closely following the flux dependence for both  $N_2$  reduction and the formation of the  $N_2$ -dependent EPR signal (Figure 5). In the presence of a saturating level of  $N_2$  (1 atm), the electron flux through nitrogenase is divided between  $N_2$  reduction and proton reduction, with at least 25% of the total flux going to proton reduction (10). It was of interest to establish the rate of  $H_2$  formation as a function of the electron flux in the presence of  $N_2$  (Figure 5). This rate is decreased by the presence of  $N_2$  but also increases as a function of flux up to the 10:1 Fe protein:MoFe protein ratio. Importantly, the distribution of electrons flowing through nitrogenase between  $N_2$  and proton reduction remains roughly constant at  $\sim 25\%$  over the flux range used here to trap the  $N_2$ -dependent EPR signal.

The intensity of the  $N_2$ -dependent EPR signal also varied with the interval between initiation of the reaction and freeze trapping at 77 K, and with the rate of freezing. The maximum EPR signal intensity was observed when the turnover sample was frozen  $\sim 15$  s after initiation of the reaction. When samples were trapped either by being frozen after reaction for only a few seconds or after reaction for several minutes, the resting-state FeMo cofactor EPR signal dominated. Optimizing the rate of freezing also maximized the intensity of the  $N_2$ -dependent EPR signal.

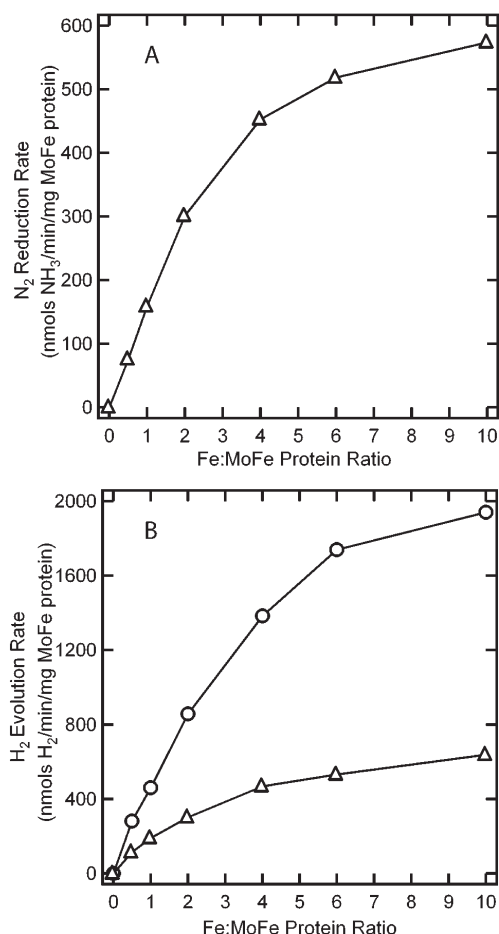


FIGURE 5: Electron flux control of nitrogenase. (A) Specific activity for ammonia formation (nanomoles of NH<sub>3</sub> formed per minute per milligram of MoFe protein) under 1 atm of N<sub>2</sub> as a function of the Fe protein:MoFe protein ratio. (B) Specific activity for H<sub>2</sub> formation (nanomoles of H<sub>2</sub> formed per minute per milligram of MoFe protein) under 1 atm of argon (O) or 1 atm of N<sub>2</sub> (Δ) as a function of the Fe protein:MoFe protein ratio. Assay conditions are described in Materials and Methods.

Fast freezing (<1 s) was achieved by initiating the turnover sample directly in the EPR tube and freezing the tube by plunging the tube into a slurry of solid and liquid hexanes frozen with liquid nitrogen, rather than liquid nitrogen alone.

When the MoFe protein was trapped under optimal conditions of pH, flux, N<sub>2</sub> partial pressure, and freeze time, the EPR signal intensity corresponded to ~20% of the resting-state FeMo cofactor EPR signal as determined by signal integration with comparison to a CuEDTA spin standard. The remainder of the FeMo cofactor had been converted to EPR-silent states that must be reduced by an odd number of electrons relative to the resting (M<sup>N</sup>) state.

**EPR Relaxation.** The intensity of the N<sub>2</sub>-dependent EPR signal at a low microwave power (50 μW) was found to increase linearly with the inverse of the temperature as expected for an energetically isolated  $S = 1/2$  state (Figure S1 of the Supporting Information). Similar behavior is seen for the hydrazine-, diazene-, and methyldiazene-trapped states (24, 31). However, spin relaxation at 4.7 K differs in the several  $S = 1/2$  states of the FeMo cofactor. The N<sub>2</sub> EPR signal intensity depended linearly on the square root of the microwave power, indicating that the onset of saturation is not reached even at the highest applied power, following the same behavior seen for the  $S = 3/2$  resting-state

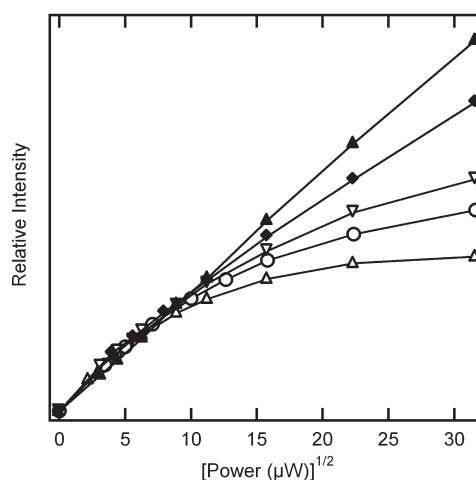


FIGURE 6: Dependence of trapped-state EPR signal intensity on the square root of the microwave power. Shown are the relative intensities of the EPR signals for the resting state (▲) or the turnover-trapped states with hydrazine (○), diazene (▽), methyldiazene (Δ), or N<sub>2</sub> (◆) as the substrate plotted vs the square root of the microwave power. Conditions are described in Materials and Methods.

FeMo cofactor (Figure 6). In contrast, a nonlinear response is seen for the hydrazine-, diazene-, and methyldiazene-trapped  $S = 1/2$  states (24, 31), which reflects the onset of saturation and longer electron spin–lattice relaxation time.

**<sup>15</sup>N and <sup>1</sup>H ENDOR.** In our preliminary report on the N<sub>2</sub>-dependent EPR signal, <sup>15</sup>N<sub>2</sub> was trapped during turnover and analysis by <sup>15</sup>N ENDOR confirmed a <sup>15</sup>N spin was coupled to the FeMo cofactor (22). This established that the novel N<sub>2</sub>-dependent EPR signal was not the result of a perturbation of the electronic properties of the FeMo cofactor as a result of N<sub>2</sub> binding elsewhere on the protein, but rather binding of N<sub>2</sub> or a reduction product to the FeMo cofactor. This study showed no evidence of the resolved <sup>1</sup>H signals expected for a –NH<sub>x</sub> moiety bound to the FeMo cofactor, in contrast to intermediates trapped during turnover of hydrazine, methyldiazene, or diazene. To more fully characterize the N<sub>2</sub>-derived species bound to the FeMo cofactor, Q-band <sup>1</sup>H CW ENDOR spectra were collected from the intermediate prepared in a H<sub>2</sub>O/D<sub>2</sub>O solution and <sup>15</sup>N-pulsed Mims ENDOR spectra were collected from the intermediate produced in H<sub>2</sub>O with <sup>15</sup>N<sub>2</sub> as the reactant.

A 2D field-frequency pattern of Q-band Mims pulsed <sup>15</sup>N ENDOR spectra was collected from the <sup>15</sup>N<sub>2</sub>-derived intermediate at multiple fields across the EPR envelope; Figure 7 shows selected spectra from this pattern. Each spectrum shows two branches centered at the <sup>15</sup>N Larmor frequency and derived from the N<sub>2</sub> substrate, as shown by comparison between spectra of intermediates prepared by turnover using either <sup>15</sup>N<sub>2</sub> or <sup>14</sup>N<sub>2</sub>. The branches are separated by a <sup>15</sup>N hyperfine coupling ( $A$ ) of ~1 MHz, roughly half those of the hydrazine, methyldiazene, and diazene intermediates (24, 31, 32). <sup>14</sup>/<sup>15</sup>N spectra collected over a wider frequency range (not shown) revealed no additional signals from a substrate-derived <sup>15</sup>N with larger couplings.

Although the intermediate shows a <sup>15</sup>N signal from a <sup>15</sup>N<sub>2</sub>-derived species bound to the FeMo cofactor, the EPR spectrum of this sample also contains a contribution from the residual resting FeMo cofactor, and previous ENDOR/ESEEM studies showed that, in this state, nitrogen atoms of α-359<sup>Arg</sup> (N1) and α-356/357<sup>Gly</sup> (N2) of MoFe protein give sharp <sup>14</sup>N ENDOR signals ( $a_{iso} = 1.05$  and 0.5 MHz, respectively) near the <sup>15</sup>N Larmor frequency in spectra collected at fields close to

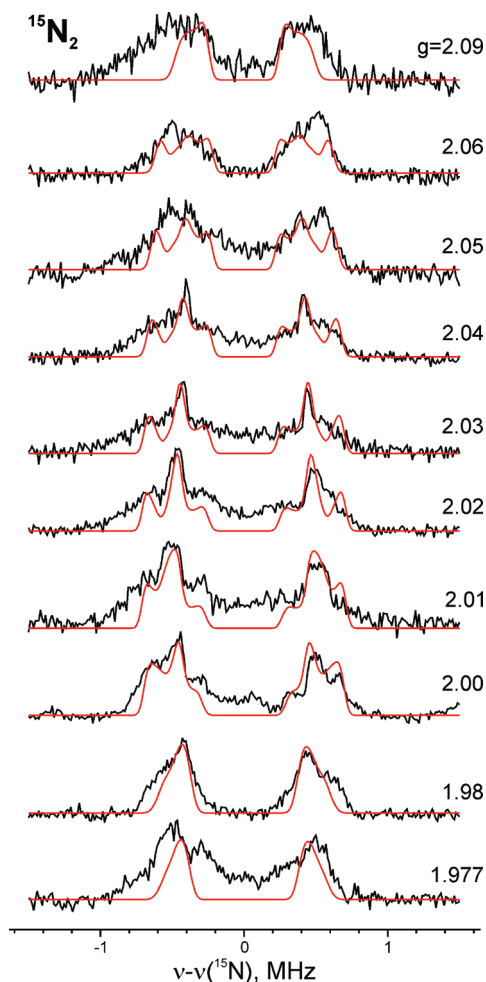


FIGURE 7: Field dependence of  $^{15}\text{N}$  Mims ENDOR for the  $^{15}\text{N}_2$ -derived intermediate in wild-type MoFe protein. Conditions: microwave frequency, 34.84 GHz; Mims sequence,  $\pi/2 = 50$  ns,  $\tau = 500$  ns; RF 40  $\mu\text{s}$ ; repetition time, 10 ms;  $\sim 1000$ – $3000$  transients/point; temperature, 2 K. Spectral baselines were corrected by simple subtraction if needed. Simulation (red) parameters:  $g = [2.08, 1.99, 1.97]$ ; hyperfine tensor  $\mathbf{A} = [0.9, 1.4, 0.45]$  MHz, Euler angles  $\alpha = 45^\circ$ ,  $\beta = 55^\circ$ , and  $\gamma = 0^\circ$  with respect to the  $g$  frame.

$g_3 = 2.00$  (33). Because of this feature, care was taken to collect background spectra from the intermediate generated by turnover using  $^{14}\text{N}_2$ . These spectra revealed  $^{14}\text{N}$  signals from the resting enzyme in the vicinity of  $\nu$  ( $^{15}\text{N}$ ), but these background resonances were found to affect the  $^{15}\text{N}$  ENDOR spectra only as a slight broadening over the low-field portion of the 2D pattern ( $g > 2.02$ ; see Figure S2 of the Supporting Information). Subtraction of these background  $^{14}\text{N}$  signals did not influence the  $^{15}\text{N}$  ENDOR line shape significantly but noticeably worsened the signal:noise ratio of the spectra. As a result, the spectra shown in Figure 7 are without correction for background, though its influence was taken into account in their simulation. The 2D  $^{15}\text{N}$  ENDOR pattern is best simulated with a hyperfine tensor,  $\mathbf{A}(^{15}\text{N}) = [0.9, 1.4, 0.45]$  MHz (Figure 7), that is dominated by its isotropic component, indicating that it arises from through-bond spin delocalization to nitrogen:  $\mathbf{A}(^{15}\text{N}) = a_{\text{iso}}\mathbf{1} + \mathbf{T} = 0.911 + [0, +0.45, -0.45]$  MHz.

X-Band ESEEM measurements to determine the  $^{14}\text{N}$  quadrupole coupling constant for the substrate-derived trapped species were attempted by a comparison of the modulations for the  $^{14}\text{N}$  and  $^{15}\text{N}$  intermediates (we know the  $^{14}\text{N}$  hyperfine tensor through simple scaling of the  $^{15}\text{N}$  tensor). Although such studies

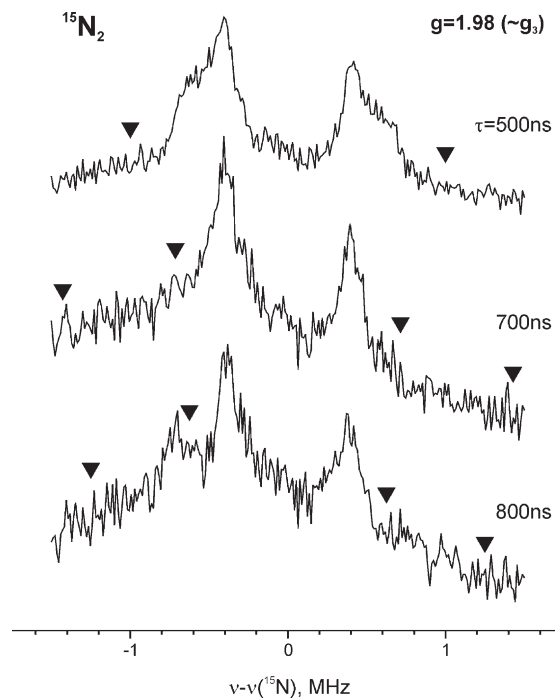


FIGURE 8:  $\tau$  dependence of ENDOR spectra collected at  $g_3$  for the  $^{15}\text{N}_2$  intermediate in wild-type MoFe protein. The triangles represent the Mims blind spots. Conditions: microwave frequency, 34.828 GHz; Mims sequence,  $\pi/2 = 50$  ns; RF 40  $\mu\text{s}$ ; repetition time, 10 ms; 1000–2000 transients/point; temperature, 2 K.

are hampered by the low intensity of the EPR signal and by low  $^{14}\text{N}$  modulation depths, analysis of ESEEM spectra collected at  $g = 2.07$  (not shown) yields estimates of the quadrupole splitting parameter and rhombicity:  $e^2qQ = 2$  MHz;  $\eta < 0.3$ .

As no  $^{14}/^{15}\text{N}$  signals derived from  $\text{N}_2$  are seen with a larger hyperfine coupling, the possibility of an additional  $^{15}\text{N}$  signal with smaller couplings was tested by collecting spectra at each of the principal  $g$  values as the duration between the first and second microwave pulses of the Mims sequence was progressively lengthened to  $\tau = 700$ – $800$  ns. This approach progressively enhances the sensitivity to smaller and smaller couplings, as described in Materials and Methods, and as illustrated in a previous  $^{13}\text{C}$  study of the intermediate formed during reduction of propargyl alcohol (17, 34). Figure 8 presents a representative set of such  $^{15}\text{N}$  spectra collected at  $g_3$ ; this field was chosen because it represents a single-crystal-like orientation and is not distorted by a contribution from background  $^{14}\text{N}$  intensity from the resting state of MoFe protein. Even at the maximum interval of  $\tau = 800$  ns there is no sign of the emergence of a doublet with a smaller  $A(^{15}\text{N})$ . Typically, such negative evidence is taken to imply a hyperfine coupling for a possibly undetected  $^{15}\text{N}$ : of  $A < 0.1$  MHz.

$^1\text{H}$  spectra were collected across the EPR envelope of the intermediate in  $\text{H}_2\text{O}$  and  $\text{D}_2\text{O}$  buffers and confirm the initial observations (Figure 9). At each field, the  $^1\text{H}$  spectra display a rather broad, “matrix” peak centered at the proton Larmor frequency, without resolved features. Little of this intensity is associated with exchangeable protons, and the shape of this peak is not changed by solvent exchange. The  $^2\text{H}$  ENDOR spectra show that the exchangeable protons likewise have a matrixlike character. This behavior sharply contrasts with that of the intermediates trapped during turnover with hydrazine, methyl-diazene, and diazene, all of which exhibit  $^1\text{H}$  spectra resolved as a doublet signal from an exchangeable proton(s)



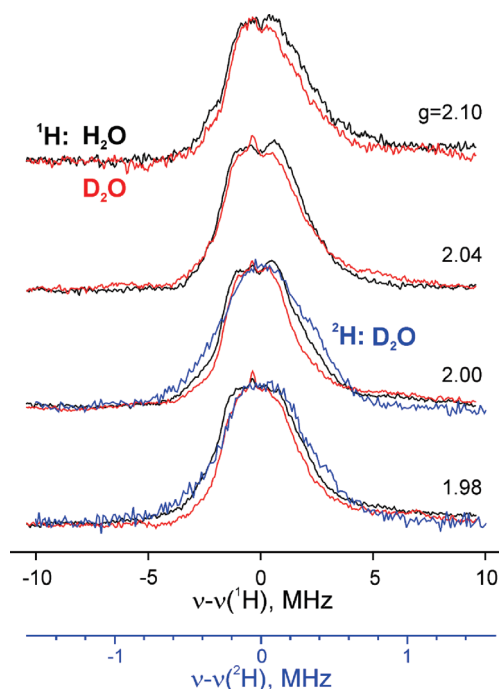


FIGURE 9: Field dependence of CW  $^1\text{H}$  ENDOR. Shown are the  $^1\text{H}$  CW ENDOR and  $^2\text{H}$  Mims ENDOR spectra for wild-type MoFe protein trapped during turnover with  $\text{N}_2$  in  $\text{H}_2\text{O}$  (black) and  $\text{D}_2\text{O}$  (red and blue) buffers. Conditions for CW ENDOR: microwave frequency, 35.096 GHz ( $\text{H}_2\text{O}$ ) and 35.083 GHz ( $\text{D}_2\text{O}$ ); modulation amplitude, 2 G; time constant, 32 ms; RF sweep speed, 1 MHz/s; bandwidth of RF broadened to 100 kHz; temperature, 2 K. Conditions for the Mims sequence: microwave frequency, 34.834 GHz;  $\pi/2 = 50$  ns,  $\tau = 500$  ns; RF 40  $\mu\text{s}$ ; repetition time, 20 ms; 100–200 transients/point; temperature, 2 K.

$[A(g_1) \sim 8\text{--}9\text{ MHz}]$ , superimposed on the matrix ENDOR peak, and assigned to an  $[-\text{NH}_x]$  fragment. Given that the  $^{14/15}\text{N}$  couplings of the  $\text{N}_2$  intermediate are roughly half of those for intermediates trapped with reduced forms of  $\text{N}_2$ , if such a fragment existed for the  $\text{N}_2$  intermediate, its  $^1\text{H}$  signal might lie within the  $^1\text{H}$  matrix pattern. However, we would expect the corresponding  $^2\text{H}$  signal to be better resolved because the matrix  $^2\text{H}$  signal would not contain contributions from the majority, nonexchangeable protons, yet no such signal is observed. Thus, the measurements support the view that the  $\text{N}_2$ -derived species bound to the FeMo cofactor is not bound by a  $[-\text{NH}_x]$  fragment.

## DISCUSSION

**Trapping the  $\text{N}_2$  State.** Freeze trapping nitrogenase during turnover with the physiological substrate  $\text{N}_2$  has revealed an EPR active state ( $S = 1/2$ ) whose intensity is found to be strongly dependent on several parameters. The need to fully optimize these parameters to yield a reasonably populated species can explain why it has not been reported in earlier studies. Among the critical parameters is the electron flux of nitrogenase. The typical turnover conditions for nitrogenase utilize a high electron flux, with a high ratio of Fe protein to MoFe protein ( $>10:1$  Fe protein:MoFe protein). The problem with such conditions for the observation of this intermediate is that an excess of reduced Fe protein is present. The reduced Fe protein  $[4\text{Fe-4S}]^+$  cluster is an  $S = 1/2$  state with an EPR signal in the  $g = 2.0$  region. The presence of this Fe protein EPR signal obscures the  $S = 1/2$  signal in the  $g = 2.0$  region of the  $\text{N}_2$ -trapped state. At low electron flux ( $<1:1$  Fe protein:MoFe protein), the  $\text{N}_2$  trapped-state EPR

signal is found to have a low intensity, making it difficult to detect. Thus, an optimal electron flux for maximal  $\text{N}_2$ -trapped state observation by EPR is found for Fe protein:MoFe protein ratios between 1:1 and 4:1. From kinetic studies, it is proposed that  $\text{N}_2$  binds to more reduced states of the MoFe protein (called the  $\text{E}_3$  and  $\text{E}_4$  states in the Thorneley and Lowe model) (27). Thus, for  $\text{N}_2$  to bind to the MoFe protein, a sufficiently high electron flux through nitrogenase must be achieved to populate the  $\text{E}_3$  and  $\text{E}_4$  states while not allowing build up of the obscuring Fe protein in its reduced state.

It was important to establish that  $\text{N}_2$  is being effectively reduced to ammonia at the electron fluxes found here to optimize the  $\text{N}_2$ -trapped state. A lack of  $\text{N}_2$  reduction to ammonia at these fluxes might indicate that the bound state is a dead-end species rather than a state along the reaction pathway. We find that at the electron flux ratios utilized here (1:1 to 4:1 Fe protein:MoFe protein) that nitrogenase does retain significant reduction rates of  $\text{N}_2$ , from 30 to 80% of the maximum rate observed at the highest electron flux. This result establishes that  $\text{N}_2$  is actually reduced to ammonia under these flux conditions. Further, an analysis of the  $\text{H}_2$  evolution rate reveals that the partitioning of electrons between reduction of  $\text{N}_2$  and protons remains roughly constant over the electron fluxes employed, indicating there are no major perturbations in the electron allocation mechanism.

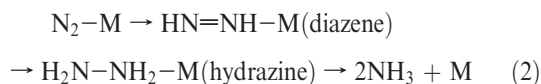
Two additional parameters were found to strongly influence the intensity of the  $\text{N}_2$ -trapped state: the time of freezing after initiation of the reaction and the rate of freezing. When turnover samples were frozen quickly after initiation of turnover conditions ( $\sim 2$  s), the intensity of the  $\text{N}_2$  trapped-state EPR signal was very low. When the sample was frozen 10 s after initiation of turnover, the signal was maximized, whereas if the sample was trapped significantly more than 10 s after initiation of turnover ( $>2$  min), the signal intensity was much lower. From the time dependence observed thus far, it is evident that a steady-state turnover condition must be achieved to maximize the  $\text{N}_2$ -derived state. Given an approximate turnover number for nitrogenase under these conditions of  $1\text{ s}^{-1}$ , the enzyme should have achieved steady-state turnover conditions at the freezing time of 10 s. At longer times, some component of the turnover reaction can become limiting (e.g., ATP or dithionite), which would result in a lower concentration of the  $\text{N}_2$ -trapped state.

How fast the sample was frozen was also found to strongly influence the intensity of the  $\text{N}_2$ -derived EPR signal. When the turnover samples were frozen by immersion of EPR tubes into liquid nitrogen over 10–15 s (slow freezing to prevent tubes from cracking), the intensity of the  $\text{N}_2$ -derived EPR signal was found to be very low or undetectable (data not shown). The  $\text{N}_2$ -derived EPR signal was observed when the sample was frozen more quickly, by rapid immersion into a slurry of hexanes and liquid nitrogen. EPR tubes can be plunged into such a slurry without cracking, and this procedure results in the rapid ( $<1$  s) freezing of the sample. Such rapid freezing proved to be critical to maximizing the signal intensity of the  $\text{N}_2$ -derived state.

The dependence of the EPR signal intensity on the concentration (partial pressure) of  $\text{N}_2$  mirrored the concentration dependence on the rate of  $\text{N}_2$  reduction to ammonia. This observation further suggests that the EPR-active  $\text{N}_2$ -derived state is trapped along the normal  $\text{N}_2$  reduction pathway. If it were not part of the pathway, a different dependence on the  $\text{N}_2$  concentration for the trapped state and the  $\text{N}_2$  reduction might be expected.

**Comparison to Other Species Trapped on Nitrogenase.** The reduction of  $\text{N}_2$  by nitrogenase is expected to occur by the

stepwise addition of electrons and protons to an  $N_2$  that remains bound to one or more metals (M) of the FeMo cofactor. If the substrate is alternately hydrogenated at the two nitrogens of  $N_2$ , rather than progressively at the “distal” nitrogen (3), two of the intermediates would be species at the level of reduction of a metal-bound diazene and metal-bound hydrazine (eq 2).



On the basis of these expected intermediates and with the goal of trapping different states along the  $N_2$  reduction pathway, we previously focused on hydrazine- and diazene (or methyldiazene)-derived states bound to the FeMo cofactor (24, 31, 32). To trap each of these nitrogenous compounds bound to the FeMo cofactor in an EPR active state, it was necessary to substitute a single amino acid near the FeMo cofactor ( $\alpha$ -70<sup>Val</sup>) to the smaller side chain amino acid Ala to allow the compounds to become effective substrates (28). Further, it was found that to trap each at reasonable concentrations, it was necessary to substitute  $\alpha$ -195<sup>His</sup> with Gln, which is thought to disrupt the flow of protons to the active site for nitrogenous substrate reduction (35). In these doubly substituted MoFe proteins, it was possible to freeze trap EPR-active intermediates during turnover of each of the three nitrogenous substrates (diazene, hydrazine, and methylhydrazine). Each is an  $S = 1/2$  spin state with an EPR signal in the  $g \sim 2$  region. Although all of these trapped states have spreads in their  $g$  values similar to that of the  $N_2$ -trapped state, each intermediate has a unique set of  $g$  values.

As part of an assessment of the similarities and differences between the  $N_2$ -trapped state and the hydrazine- and diazene-trapped states, the pH dependence on the intensity of the trapped-state EPR spectrum was determined for each substrate (Figure 2). The  $N_2$ -trapped state shows a different pH dependence when compared to that observed for the hydrazine-, diazene-, and methyldiazene-trapped states. Further, the microwave power dependence of the EPR signal intensities for each trapped state is different (Figure 6). It was found that the signal intensity of the resting-state FeMo cofactor and that of the  $N_2$ -trapped state both show a linear dependence of signal intensity on the square root of the microwave power, indicating that these signals do not saturate at 10 K under the highest available microwave power. In contrast, at 10 K the hydrazine, diazene, and methyldiazene signals all show saturation, indicating that they have longer electron-spin relaxation times.

**$N_2$ -Trapped State.** The observation that the  $N_2$ -trapped state exhibits a  $^{15}N$  ENDOR signal whose hyperfine tensor is dominated by its isotropic term establishes that a  $N_2$ -derived species is covalently bound to the  $S = 1/2$  FeMo cofactor of this intermediate. Analogous signals were observed with the intermediates trapped during turnover with hydrazine, methyldiazene, and diazene. The absence of a resolved  $^{1/2}H$  signal from exchangeable proton(s) contrasts with the intermediates trapped with these other substrates, each of which exhibits both a  $^{15}N$  ENDOR signal from substrate and a signal from an exchangeable proton(s) with  $A(g_1) \sim 8\text{--}9$  MHz (24, 31, 32). As the simultaneous observation of the  $^1H$  and  $^{15}N$  signals suggests the presence of a substrate-derived  $[-NH_x]$  moiety bound directly to the FeMo cofactor, the absence of a  $^1H$  signal from the  $N_2$ -trapped state suggests that this intermediate is at a distinct and earlier stage of reduction.

To consider the implications of the magnitude of  $a_{iso}$  in discriminating among potential binding geometries and identifying

the binding metal ion(s), it is noted that  $^{15}N$  bound to an exchange-coupled metal cluster has a hyperfine coupling scaled by an unknown spin-projection coefficient ( $K^i$ ) associated with the FeMo cofactor metal ion to which it binds:  $a_{iso} = K^i a_{iso}^i$  (36), where  $a_{iso}^i$  is the coupling associated with  $^{15}N$  bound to ion  $i$  in the absence of exchange coupling. By analogy to characteristics of carboxylate-bridged diiron centers, nitrogenous ligands to high-spin Fe(II) ( $S = 2$ )/Fe(III) ( $S = 5/2$ ) ions might be expected to have intrinsic isotropic hyperfine coupling constants ( $a_{iso}$ ) in the range of  $\sim 4\text{--}8$  MHz (37). The same is true for low-spin Fe(III) ( $S = 1/2$ ); while nothing is yet known about Mo(III), the value is expected to be no lower. On the basis of these considerations, there appear to be only two plausible interpretations of the small measured  $a_{iso}$  of  $\sim 1$  MHz for the FeMo cofactor-bound  $[-^{15}N]$ : (i) it binds to a paramagnetic metal ion(s) [Fe(III), Fe(I), or Mo(III)] whose spin-projection coefficient is extremely small ( $K^i < 1/5$ ), or (ii) it binds to an essentially diamagnetic metal ion(s) [Fe(II) < Mo(IV)] that acquires a small spin density through bond polarization.

The absence of an ENDOR  $^{15}N$  signal from the second  $^{15}N$  suggests an end-on binding mode. In such a case, one would expect  $a_{iso}(\text{distal})/a_{iso}(\text{proximal})$  to be no lower than  $\sim 1/10$ , which could make the ENDOR signal from the distal  $^{15}N$  undetectable, given the small coupling to the proximal  $^{15}N$  found here. Further, the provisional finding of small quadrupole-tensor rhombicity for the bound  $[-^{14}N]$  is supportive of this idea. Although a bridging mode is not ruled out at this time, the requirement of such a small coupling for the second  $^{15}N$  would dictate that it could only be bound to an effectively diamagnetic metal ion. Thus, the results presented here are consistent with the bound species being  $N_2$  bound end-on to a metal (M) of the FeMo cofactor ( $M-N\equiv N$ ). Model studies should help us to understand the types of hyperfine and quadrupole couplings to be expected for such a structure (e.g., the ratio between couplings to bound and remote N), as well as for other candidates such as  $M-N=NH$ ,  $M=N-NH_2$ , and  $M\equiv N$  (3) and thus should help confirm the structure of this intermediate.

**Summary.** In summary, parameters have been optimized for trapping a species derived from  $N_2$  bound to the active-site FeMo cofactor in the wild-type MoFe protein. Characterization of this bound state confirms the presence of a single type of N atom derived from  $N_2$  bound to the FeMo cofactor, consistent with an  $N_2$  bound end-on to one or more metal ions. Further, evidence is presented that supports the absence of an H atom added to the N atom bound to the FeMo cofactor, favoring minimal reduction of the bound  $N_2$  species.

## SUPPORTING INFORMATION AVAILABLE

Additional figures illustrating the temperature dependence of the  $N_2$ -derived EPR signal and a check for  $^{15}N$  Mims ENDOR field dependence of the  $^{15}N_2$ -derived intermediate. This material is available free of charge via the Internet at <http://pubs.acs.org>.

## REFERENCES

- Burgess, B. K., and Lowe, D. J. (1996) The mechanism of molybdenum nitrogenase. *Chem. Rev.* 96, 2983–3011.
- Seefeldt, L. C., Hoffman, B. M., and Dean, D. R. (2009) Mechanism of Mo-dependent nitrogenase. *Annu. Rev. Biochem.* 78, 701–722.
- Hoffman, B. M., Dean, D. R., and Seefeldt, L. C. (2009) Climbing nitrogenase: Toward a mechanism of enzymatic nitrogen fixation. *Acc. Chem. Res.* 42, 609–619.
- Rees, D. C., Tezcan, F. A., Haynes, C. A., Walton, M. Y., Andrade, S., Einsle, O., and Howard, J. B. (2005) Structural basis of biological nitrogen fixation. *Philos. Trans. R. Soc. London, Ser. A* 363, 971–984.



5. Shah, V. K., and Brill, W. J. (1977) Isolation of an iron-molybdenum cofactor from nitrogenase. *Proc. Natl. Acad. Sci. U.S.A.* 74, 3249–3253.
6. Howard, J. B., and Rees, D. C. (1996) Structural basis of biological nitrogen fixation. *Chem. Rev.* 96, 2965–2982.
7. Einsle, O., Tezcan, F. A., Andrade, S. L. A., Schmid, B., Yoshida, M., Howard, J. B., and Rees, D. C. (2002) Nitrogenase MoFe-protein at 1.16 angstrom resolution: A central ligand in the FeMo-cofactor. *Science* 297, 1696–1700.
8. Hageman, R. V., and Burris, R. H. (1978) Nitrogenase and nitrogenase reductase associate and dissociate with each catalytic cycle. *Proc. Natl. Acad. Sci. U.S.A.* 75, 2699–2702.
9. Burgess, B. K. (1985) Substrate reactions of nitrogenase. In *Metal Ions in Biology: Molybdenum Enzymes* (Spiro, T. G., Ed.) pp 161–220, John Wiley and Sons, New York.
10. Simpson, F. B., and Burris, R. H. (1984) A nitrogen pressure of 50 atm does not prevent evolution of hydrogen by nitrogenase. *Science* 224, 1095–1097.
11. Kim, J., and Rees, D. C. (1992) Crystallographic structure and functional implications of the nitrogenase molybdenum iron protein from *Azotobacter vinelandii*. *Nature* 360, 553–560.
12. Kim, J., and Rees, D. C. (1992) Structural models for the metal centers in the nitrogenase molybdenum-iron protein. *Science* 257, 1677–1682.
13. Chan, M. K., Kim, J., and Rees, D. C. (1993) The nitrogenase FeMo-cofactor and P-cluster pair: 2.2 Å resolution structures. *Science* 260, 792–794.
14. Christiansen, J., Cash, V. L., Seefeldt, L. C., and Dean, D. R. (2000) Isolation and characterization of an acetylene-resistant nitrogenase. *J. Biol. Chem.* 275, 11459–11464.
15. Christiansen, J., Seefeldt, L. C., and Dean, D. R. (2000) Competitive substrate and inhibitor interactions at the physiologically relevant active site of nitrogenase. *J. Biol. Chem.* 275, 36104–36107.
16. Mayer, S. M., Niehaus, W. G., and Dean, D. R. (2002) Reduction of short chain alkynes by a nitrogenase  $\alpha$ -70Ala-substituted MoFe protein. *J. Chem. Soc., Dalton Trans.* 5, 802–807.
17. Lee, H. I., Igarashi, R. Y., Laryukhin, M., Doan, P. E., Dos Santos, P. C., Dean, D. R., Seefeldt, L. C., and Hoffman, B. M. (2004) An organometallic intermediate during alkyne reduction by nitrogenase. *J. Am. Chem. Soc.* 126, 9563–9569.
18. Lee, H. I., Sørle, M., Christiansen, J., Yang, T. C., Shao, J., Dean, D. R., Hales, B. J., and Hoffman, B. M. (2005) Electron inventory, kinetic assignment (E(n)), structure, and bonding of nitrogenase turnover intermediates with  $C_2H_2$  and CO. *J. Am. Chem. Soc.* 127, 15880–15890.
19. Igarashi, R. Y., Laryukhin, M., Dos Santos, P. C., Lee, H. I., Dean, D. R., Seefeldt, L. C., and Hoffman, B. M. (2005) Trapping  $H^-$  bound to the nitrogenase FeMo-cofactor active site during  $H_2$  evolution: Characterization by ENDOR spectroscopy. *J. Am. Chem. Soc.* 127, 6231–6241.
20. Lukoyanov, D., Barney, B. M., Dean, D. R., Seefeldt, L. C., and Hoffman, B. M. (2007) Connecting nitrogenase intermediates with the  $N_2$  reduction kinetic scheme by a relaxation protocol and identification of the  $N_2$  binding state. *Proc. Natl. Acad. Sci. U.S.A.* 104, 1451–1455.
21. Thorneley, R. N. F., and Lowe, D. J. (1985) Kinetics and mechanisms of the nitrogenase enzyme system. In *Molybdenum Enzymes* (Spiro, T. G., Ed.) pp 221–284, John Wiley and Sons, New York.
22. Barney, B. M., Yang, T. C., Igarashi, R. Y., Dos Santos, P. C., Laryukhin, M., Lee, H. I., Hoffman, B. M., Dean, D. R., and Seefeldt, L. C. (2005) Intermediates trapped during nitrogenase reduction of  $N_2$ ,  $CH_3-N=NH$ , and  $H_2N-NH_2$ . *J. Am. Chem. Soc.* 127, 14960–14961.
23. Christiansen, J., Goodwin, P. J., Lanzilotta, W. N., Seefeldt, L. C., and Dean, D. R. (1998) Catalytic and biophysical properties of a nitrogenase apo-MoFe protein produced by a *nifB*-deletion mutant of *Azotobacter vinelandii*. *Biochemistry* 37, 12611–12623.
24. Barney, B. M., Laryukhin, M., Igarashi, R. Y., Lee, H. I., Dos Santos, P. C., Yang, T. C., Hoffman, B. M., Dean, D. R., and Seefeldt, L. C. (2005) Trapping a hydrazine reduction intermediate on the nitrogenase active site. *Biochemistry* 44, 8030–8037.
25. Hoffman, B. M., DeRose, V. J., Doan, P. E., Gurbel, R. J., Houseman, A. L. P., and Telser, J. (1993) Metalloenzyme active-site structure and function through multifrequency CW and pulsed ENDOR. In *Biological Magnetic Resonance* (Berliner, L. J., and Reuben, J., Eds.) pp 151–218, Plenum Press, New York.
26. Davis, L. C., and Orme-Johnson, W. H. (1976) Nitrogenase IX: Effects of the MgATP generator on the catalytic and EPR properties of the enzyme in vitro. *Biochim. Biophys. Acta* 452, 42–58.
27. Rivera-Ortiz, J. M., and Burris, R. H. (1975) Interactions among substrates and inhibitors of nitrogenase. *J. Bacteriol.* 123, 537–545.
28. Barney, B. M., Igarashi, R. Y., Dos Santos, P. C., Dean, D. R., and Seefeldt, L. C. (2004) Substrate interaction at an iron-sulfur face of the FeMo-cofactor during nitrogenase catalysis. *J. Biol. Chem.* 279, 53621–53624.
29. Fisher, K., Newton, W. E., and Lowe, D. J. (2001) Electron paramagnetic resonance analysis of different *Azotobacter vinelandii* nitrogenase MoFe-protein conformations generated during enzyme turnover: Evidence for  $S = 3/2$  spin states from reduced MoFe-protein intermediates. *Biochemistry* 40, 3333–3339.
30. Burgess, B. K., Wherland, S., Newton, W. E., and Stiefel, E. I. (1981) Nitrogenase reactivity: Insight into the nitrogen-fixing process through hydrogen-inhibition and HD-forming reactions. *Biochemistry* 20, 5140–5146.
31. Barney, B. M., Lukoyanov, D., Yang, T. C., Dean, D. R., Hoffman, B. M., and Seefeldt, L. C. (2006) A methylidiazene ( $HN=N-CH_3$ ) derived species bound to the nitrogenase active site FeMo-cofactor: Implications for mechanism. *Proc. Natl. Acad. Sci. U.S.A.* 103, 17113–17118.
32. Barney, B. M., McClead, J., Lukoyanov, D., Laryukhin, M., Yang, T. C., Dean, D. R., Hoffman, B. M., and Seefeldt, L. C. (2007) Diazene ( $HN=NH$ ) is a substrate for nitrogenase: Insights into the pathway of  $N_2$  reduction. *Biochemistry* 46, 6784–6794.
33. Lee, H. I., Benton, P. M., Laryukhin, M., Igarashi, R. Y., Dean, D. R., Seefeldt, L. C., and Hoffman, B. M. (2003) The interstitial atom of the nitrogenase FeMo-cofactor: ENDOR and ESEEM show it is not an exchangeable nitrogen. *J. Am. Chem. Soc.* 125, 5604–5605.
34. Benton, P. M. C., Laryukhin, M., Mayer, S. M., Hoffman, B. M., Dean, D. R., and Seefeldt, L. C. (2003) Localization of a substrate binding site on FeMo-cofactor in nitrogenase: Trapping propargyl alcohol with an  $\alpha$ -70-substituted MoFe protein. *Biochemistry* 42, 9102–9109.
35. Kim, C. H., Newton, W. E., and Dean, D. R. (1995) Role of the MoFe protein  $\alpha$ -subunit histidine-195 residue in FeMo-cofactor binding and nitrogenase catalysis. *Biochemistry* 34, 2798–2808.
36. Lukoyanov, D., Pelmeshnikov, V., Maeser, N., Laryukhin, M., Yang, T. C., Noodleman, L., Dean, D. R., Case, D. A., Seefeldt, L. C., and Hoffman, B. M. (2007) Testing if the interstitial atom, X, of the nitrogenase molybdenum-iron cofactor is N or C: ENDOR, ESEEM, and DFT studies of the  $S = 3/2$  resting state in multiple environments. *Inorg. Chem.* 46, 11437–11449.
37. DeRose, V. J., Liu, K. E., Lippard, S. J., and Hoffman, B. M. (1996) Investigation of the dinuclear Fe center of methane monooxygenase by advanced paramagnetic resonance techniques: On the geometry of DMSO binding. *J. Am. Chem. Soc.* 118, 121–134.